Advanced bioceramic composite for bone tissue engineering: Design principles and structure–bioactivity relationship

Ahmed R. El-Ghannam
Tissue Engineering and Bioactive Materials Laboratory, Center for Biomedical Engineering, The Graduate School, Oral Health Science Center, School of Dentistry, University of Kentucky, Lexington, Kentucky 40506

Received 1 August 2003; revised 5 January 2004; accepted 29 January 2004
Published online 8 April 2004 in Wiley InterScience (www.interscience.wiley.com). DOI: 10.1002/jbm.a.30022

Abstract: The synthesis of a new resorbable porous bioactive silica-calcium phosphate composite (SCPC) that can be used as a tissue-engineering scaffold for bone regeneration is described. The effects of chemical composition and thermal treatment on crystallization and the mechanism of phase transformation in SCPC were evaluated. In the silica-rich samples, β-rhenanite (β-$NaCaPO_4$) and α-cristobalite (SiO_2) were the dominant phases after treatment at 800°C. On the other hand, in the calcium phosphate-rich samples, calcium pyrophosphate ($Ca_2P_2O_7$) was formed in addition to β-rhenanite and α-cristobalaite. X-ray diffraction analyses showed a shift in the 2θ value of the main peak(s) of all phases indicating the formation of solid solutions. Phase transformation reactions were accompanied by a loss of water molecules that contributed to the formation of pores in the size range 10–300 μm. All SCPC samples adsorbed a significantly higher quantity of serum protein than bioactive glass ($p < 0.0001$). In addition, the silica-rich SCPC adsorbed a significantly higher amount of serum protein than the calcium phosphate-rich samples ($p < 0.003$). While the crystallization of amorphous silica into L-quartz significantly inhibited serum protein adsorption, the transformation of L-quartz into α-cristobalite solid solution (ss) significantly enhanced protein adsorption. On the other hand, in conjunction with the transformation of brushite ($CaHPO_4$) into pyro- and tri-calcium phosphates, there was a significant decrease in protein adsorption. However, as pyro- and tri-calcium phosphates transformed into β-rhenanite, by thermal treatment, protein adsorption increased markedly. Critical-size bone defects grafted with silica-rich SCPC were filled with new bone and contained minimal residues of the graft material. Bone defects grafted with bioactive glass enhanced new bone formation, however, with very limited resorption. The enhanced resorption of SCPC *in vivo* correlates well with the higher rate of silica dissolution from SCPC than bioactive glass. The facilitated Si dissolution was associated with rapid bone regeneration in defects grafted with SCPC. The enhanced bioactivity properties of the SCPC are due to its chemical composition, modified crystalline structure, and high porosity. The new SCPC may be used for a wide variety of applications in the field of bone reconstruction including tissue-engineering scaffolds for cell and drug delivery. © 2004 Wiley Periodicals, Inc. J Biomed Mater Res 69A: 490–501, 2004

Key words: silica-calcium phosphate composite; mechanism of phase transformation; protein adsorption; bone generation; synthetic graft resorption

INTRODUCTION

Tissue loss as a result of injury or disease, in an aging population, provides reduced quality of life for many at a significant socioeconomic cost.[1] Annually, there are approximately 6.5 million bone fractures in the US.[2] Enhanced bone regeneration is essential for healing large bone defects secondary to tumor or trauma, and for treating fracture-delayed unions or nonunions, which constitute 10–15% of the fractures.[3] Approaches to these difficult bone repair problems include utilization of autografts, allografts, and synthetic grafts.[4] Although autograft material is currently the material of choice, there are limitations associated with its use, including donor site morbidity, limited donor bone supply, anatomical and structural problems, and elevated levels of resorption during healing.[5] The use of allografts has the disadvantage of eliciting an immunological response due to genetic differences and the risk of inducing transmissible diseases.[5,6]

Calcium phosphate ceramics and bioactive glasses were introduced more than 30 years ago as bone substitutes. These materials are considered bioactive because they bond to bone and enhance bone tissue formation. The forms of calcium phosphate ceramics most widely used are tricalcium phosphate (Ca_3

Correspondence to: A.R. El-Ghannam; e-mail: arelgh2@uky.edu

$[PO_4]_2$, TCP Whitlockite), and hydroxyapatite $[Ca_{10}(PO_4)_6(OH)_2]$ (HA). These materials have a similar structure to the mineral phase of bone and have been shown to be osteoconductive, i.e., enhance bone cells growth and direct bone deposition on their surfaces. The availability of HA and TCP in porous shapes has encouraged many investigators to evaluate the ability of these biomaterials to serve as tissue engineering scaffolds for cell and drug delivery. However, there are problems associated with inflammatory and immunologic reactions and disease transmission when used as carriers for osteoinductive factors.[7–9] Moreover, although evidence of bone growth in porous and dense HA particulates is widespread, the bone conductive effect is limited.[10] Often at a distance away from the bone defect wall, these particulates are encapsulated by fibrous tissue. TCP is more biodegradable than HA; however, its presence elicits a foreign body response.[11] Bioactive glass (BG), which contains (45 wt %) of silica in addition to calcium and phosphorous, is known to have the most stimulatory effect on bone cell function.[10,12–17] When implanted in bone, BG accelerated bone growth three times more than HA.[18] However, BG is a solid non-resorbable material.[19] A suitable macro porous structure is necessary to obtain good implant incorporation through rapid vascularization and bone ingrowth.[20–22] Unfortunately, there is a limited opportunity to synthesize a porous BG and improve its mechanical and physicochemical properties without decrements in bioactivity.

The rapid bone bonding to BG was associated with the rapid formation of a calcium-deficient carbonate-containing hydroxyapatite (HCA) layer on the material surface. Immersion of BG in simulated body fluid (SBF) (with ion concentrations similar to the interstitial fluid) resulted in the formation of a surface HCA similar to that observed *in vivo*. The mechanism of formation of this layer includes a series of chemical reactions that occur within a controlled sequence: leaching, dissolution, and precipitation.[23–29] After leaching and dissolution, the glass surface is covered with a silica gel layer rich in silanol (Si-OH) groups. The Si-OH groups nucleate the crystallization of a HCA layer at the surface of BG.[24–27] Accordingly, the HCA layer, which is a prerequisite for bone bonding, is still incorporating silica that could be an important reason for the strong stimulatory effect on bone tissue formation. However, a major drawback of the silica-rich layer is that it slows down BG dissolution by inhibiting ion diffusion from the glass bulk into the surface. The implication for the slow rate of dissolution of BG is the slow rate of resorption *in vivo*. Moreover, in the presence of serum protein, the HCA layer did not form on the BG surface most probably because the protein molecules chelate the Ca ions necessary for the HCA layer formation.[14,15]

Consequently, bone cells *in vivo* may interact with the silica-rich layer, which may contain calcium and phosphorus either as substituted ions in the silica network or as amorphous accumulates but not necessary as an HCA layer. As such, we theorize that a silica-based calcium phosphate composite would optimally enhance bone cell function. This study reports on the synthesis and characterization of a new, resorbable, porous, bioactive silica-based calcium phosphate composite (SCPC) that has the ability to stimulate rapid bone generation and resorb when grafted in large bone defects. To enhance bioactivity and resorbability, ion substitution and formation of solid solution were induced in the crystalline phases. Thus, the entire structure of SCPC contains unmodified silica, ion substituted silica, unmodified calcium phosphate, and calcium phosphate modified with Na and/or silica. These four different regions will synergistically enhance bioactivity and resorbability of the material. Figure 1 is a schematic that describes the morphology of a cross-section of BG covered with HCA layer and that of the new porous SCPC. While the resorption and bioactivity of BG is limited by ion diffusion from the glass bulk to the surface, the resorption and bioactivity of the SCPC do not depend on the bulk composition. The modified calcium phosphate phases can work as a weak binder for the modified silica phases and offer sites for preferential dissolution. The role of silica is threefold: silica substitution in the calcium phosphate mineral regulates its resorption and enhances its bioactivity. Second, the silica surface, which was not incorporated in the calcium phosphate, can nucleate the precipitation of a carbonated hydroxyapatite bioactive layer on the composite surface. Third, Ca and P can be incorporated in the silica network itself, Ca as network modifier and P as network former, and create a surface with activity superior to that of BG. The aim of the present work is to evaluate the effect of chemical composition and thermal treatment on the crystallization behavior of the silica and calcium phosphate phases. The composition and crystalline structure of the new graft material were correlated to serum protein adsorption, Si corrosion, bone tissue generation, and graft material resorption. The bioactivity of the new SCPC was compared to that of BG.

MATERIALS AND METHODS

Composite preparation

Table I shows the chemical composition of different silica-containing calcium phosphate ceramics (C1S3, C1S1, and C3S1) used in this study. Appropriate ratios of dicalcium phosphate $CaHPO_4 \cdot 2H_2O$ and silicon components were placed in polyethylene bottles and mixed on a roller mixer

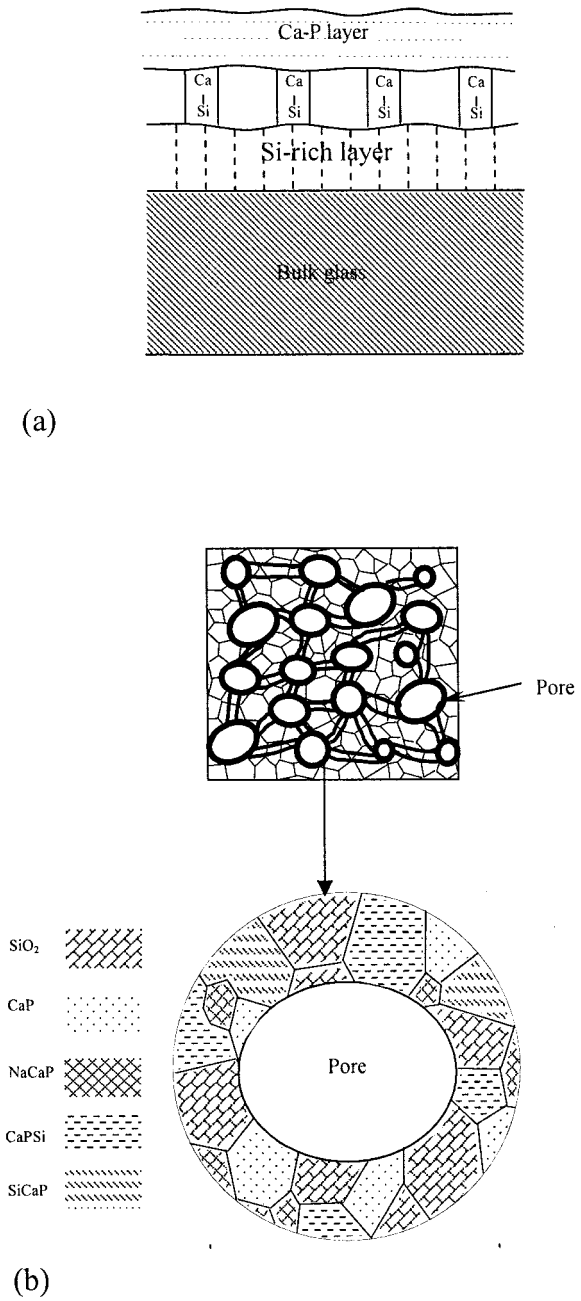

Figure 1. (a) A schematic diagram of a cross-section of bioactive glass showing the calcium phosphate-rich layer, the silica-rich layer, and the interface between the two layers. The silica-rich layer slows down BG dissolution by inhibiting ion diffusion from the glass bulk into the surface. The implication for the slow rate of dissolution of BG is the slow rate of resorption *in vivo*. (b) Schematic of the cross-section of silica-calcium phosphate composite (SCPC) showing that the entire structure is based on interconnected phases of modified silica and calcium phosphate minerals. The bioactivity and resorbability of these phases are induced by enforcing ion substitution and formation of solid solutions. The porosity of the new SCPC provides high surface area for protein adsorption, cell adhesion, and new bone formation. The unique chemical composition, modified crystalline structure, and the porosity of SCPC work out synergistically to enhance material resorbability and bone bioactivity.

TABLE I
Composition in Mol % of Silica-Calcium Phosphate Composites

Sample notation	CaO	SiO_2	P_2O_5	Na_2O
C1S3	10.1	63.7	5.0	21.2
C1S1	23.2	49.0	11.5	16.3
C3S1	40.6	29.2	20.5	9.7

for 24 h. Each batch was moistened with 0.1 NaOH and placed in a teflon mold 10 mm diameter × 10 mm height. The samples were left to dry at room temperatures and then thermally treated at 130, 180, 355, 690, or 800°C. The sintering temperatures were selected based on the differential thermal analysis results shown below.

Thermal analysis

Differential thermal analysis (DTA) was employed to determine the temperatures at which crystallization and phase transformation occurred. The weight losses associated with crystal formation or phase transformation during heating were analyzed by differential thermo-gravimetric analysis (DTGA). Powdered samples of grain size range 90–250 μm from each composition were heated in the temperature range 50–900°C with a heating rate 20°C/min using computerized 7 series USA PerkinElmer thermal analysis system. The material was analyzed using aluminum oxide powder as a reference.

Heat treatment

To study the effect of chemical composition and temperature on the mechanism of phase transformation, SCPC samples were subjected to a single-step heat-treatment in air at 130, 180, 355, 690, or 800°C for 2 h at a heating rate of 2°C/min. These temperatures were selected based on the maxima of the peaks recorded in the DTA analyses.

X-ray diffraction analysis (XRD)

XRD was used to identify the crystalline phases formed in SCPC after each heat-treatment. Samples of grain size <38 μm were analyzed using Philips diffractometer (type PW 1390, Philips Electronic Instruments, Eindhoven, The Netherlands) employing Ni-filtered Cu Kα irradiation at 40 Kv and 25 mA.

Scanning electron microscopy

To analyze the morphology and porosity, thermally treated samples were coated with gold and were analyzed using an electron microscope (Model XL30; Philips Elec-

tronic Instruments) at 20 kV. In addition, the porosity percent and pore size range were analyzed by mercury intrusion technique (Micromeretics Corporation, Norcross, GA).

Protein adsorption

To evaluate the effect of chemical composition and crystalline structure of SCPC on serum protein adsorption, particles (90–250 μm) from each composite were separately immersed in simulated body fluid (tris buffer supplemented with ions in concentration similar to the interstitial fluid, SBF) containing 10% fetal bovine serum for 1 h at 37°C. For comparison, protein adsorption onto BG particles of the same size range was evaluated. After immersion, the samples were washed with tris buffer solution (pH 7.2) to remove unattached protein. Adsorbed protein was extracted using 1% sodium dodecyle sulfate solution (SDS), pH 7.4. Protein concentration in the extract was determined using a gold staining dot blot technique. The extracted protein was diluted with SDS (1:7) and micropipetted onto a nitrocellulose sheet (NC) (BA-85, 0.45 μm pore size, Schleicher and Schuell Inc., Keen, NH). The NC paper was air-dried, blocked in 3% Tween-20 solution for 30 min, and stained with gold staining. The protein dots were digitized and their intensities were measured using Gel pro software. The concentration of the adsorbed protein was calculated using a bovine serum albumin calibration curve.

Corrosion analysis

To compare the rate of corrosion of SCPCs and BG, 0.3-g particles (90–250 μm) of each material were immersed in 5 ml of tissue culture medium (α-MEM) containing 10% serum, at 37°C, for 1, 2, 4, 6, or 8 days. After each time period, the medium was collected and the ionic concentration of Si was measured using Inductively Coupled Plasma Optical Emission Spectrometer (Optima 3000 ICP-EMS, PerkinElmer). Si corrosion was selected to represent the degradation of the material because silica constitutes the main component of C1S3 and BG. Three replications per time period per each material were evaluated.

Animal study

In a pilot study, bone tissue response to the new SCPC material was evaluated using the rabbit femur model. Nine (9) rabbits 3–4 months weighing about 3 kg were divided into three groups ($n = 3$). Each group was grafted with one kind of graft material. A critical size bone defect (6 mm in diameter) was created in the cortical bone of each femur. Granules (150–600 μm) of C1S3 and C3S1, both pretreated at 690°C, as well as control BG of the same particle size were used separately in sufficient amounts to fill the defects. The animals were sacrificed after 3 weeks. Bone segments containing the defects were fixed, dehydrated, decalcified, sliced into thin sections (5–7 μm), and stained with H & E.

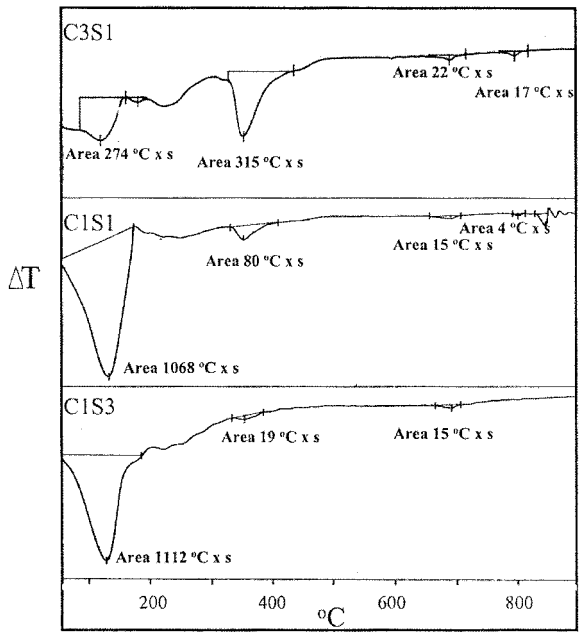

Figure 2. Differential thermal analysis of various silica-calcium phosphate composites. The samples were heated in the temperature range 50–850°C with a heating rate of 20°C/min. Al_2O_3 powder was used as a reference. All samples showed three endothermic peaks around 125, 353, and 690°C. The area under the peak centered at 125°C increased in the order C1S3 > C1S1 > C3S1. Reversibly, the area under the peak centered at 353°C decreased in the order C1S3 < C1S1 < C3S1.

Statistical analysis

Statistical analyses of the protein adsorption and corrosion data were analyzed by one-way analysis of variance (ANOVA) using a SigmaStat program (Student-Newman-Kuels). The level of significance was defined at 95%.

RESULTS

Thermal analysis

DTA

Differential thermal analyses of C3S1, C1S1, and C1S3 samples are shown in Figure 2. All samples showed three endothermic peaks around 125, 353, and 690°C. The area under the peak centered at 125°C increased in the order C1S3 > C1S1 > C3S1. Reversibly, the area under the peak centered at 353°C decreased in the order C1S3 < C1S1 < C3S1. The thermogram of the calcium phosphate-rich composite (C3S1) showed an additional small peak at 796°C. The area of that peak decreased to a minimum and totally disappeared in the thermogram of C1S1 and C1S3, respectively.

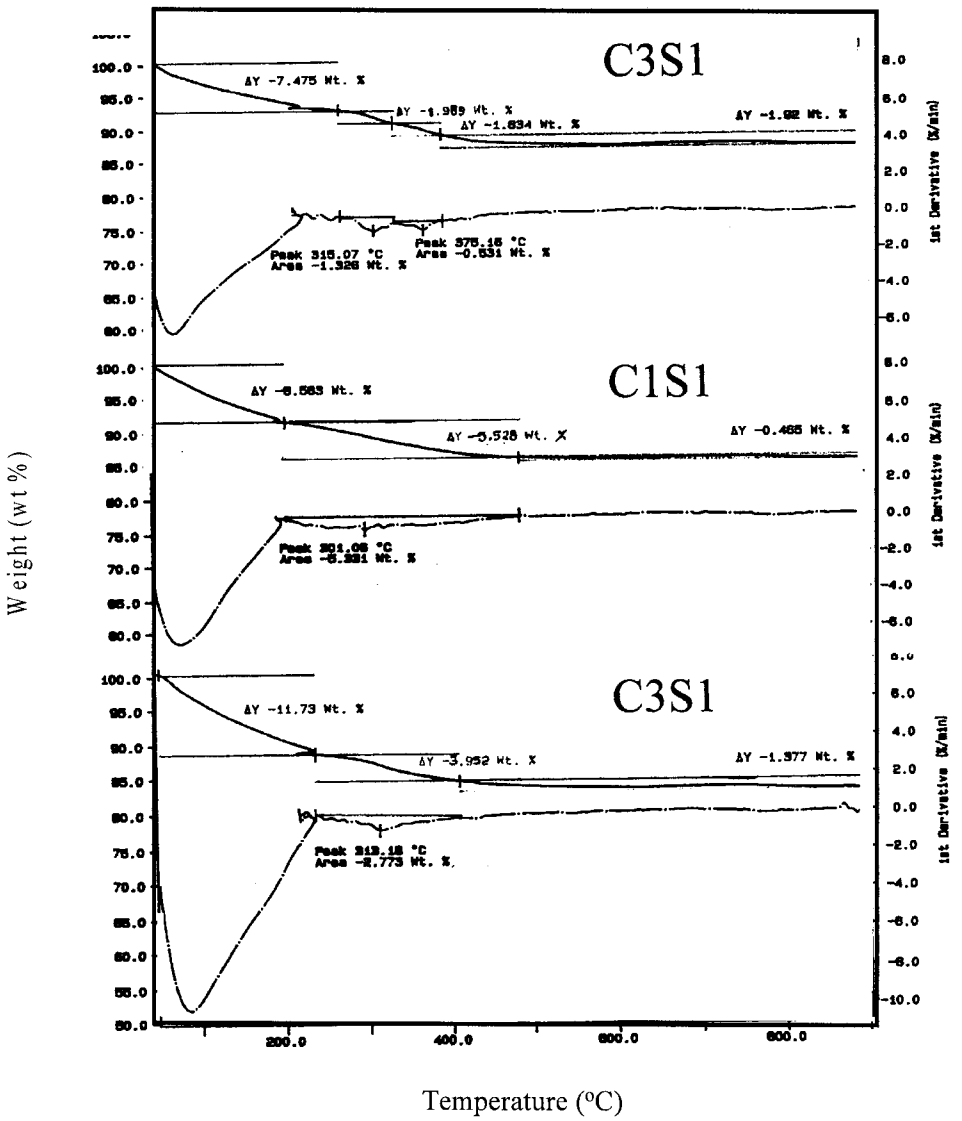

Figure 3. Thermo-gravimetric analyses of samples C3S1, C1S1, and C1S3. A major weight loss, in the temperature range 50–200°C, is shown, which was increased as the percentage of the silica component was increased. Thus, C1S3, C1S1, and C3S1 lost 11.73, 8.58, and 7.47% respectively. In the temperature range 200–400°C; comparable weight losses among the samples were recorded. However, while the weight loss took place in one step for C1S1 and C1S3, the weight loss in the C3S1 took place in two distinct steps centered at 315° and 375°C.

DTGA

Figure 3 shows the DTGA thermogram of C3S1, C1S1, and C1S3. Upon heating all samples, a major weight loss started at 50°C and continued up to 200°C. Comparison among samples indicated that the total weight loss decreased in the order C1S3 > C1S1 > C3S1. Thus, C3S1, C1S1, and C1S3 lost 7.47, 8.58, and 11.73%, respectively. However, in the temperature range 200–400°C; C3S1, C1S1, and C1S3 lost 3.95, 5.5, and 3.8%, respectively. It is worthy to note that while the weight loss in this temperature range took place in one-step for C1S1 and C1S3, the weight loss in the C3S1 took place in two distinct steps centered at 315 and 375°C. In the temperature range 400–850°C; C3S1, C1S1, and C1S3 lost 1.37, 0.46, and 1.9 wt %, respectively.

X-ray diffraction analysis

C1S3

C1S3 treated at 130° or 180°C comprised mainly brushite ($CaHPO_4$), L-quartz (SiO_2) (ss), and β-rhenanite (β-$NaCaPO_4$) (ss) (Fig. 4). There was a shift in the position of the main characteristic peaks of L-quartz and β-rhenanite, in all samples, indicating formation of solid solution. The weak signals of these phases indicate ill crystallization due to the presence of a high content of amorphous silica. Raising the treatment temperature to 355°C resulted in complete transformation of $CaHPO_4$ into β-$NaCaPO_4$ ss and L-quartz ss into α-cristobalite (SiO_2) ss. The position of

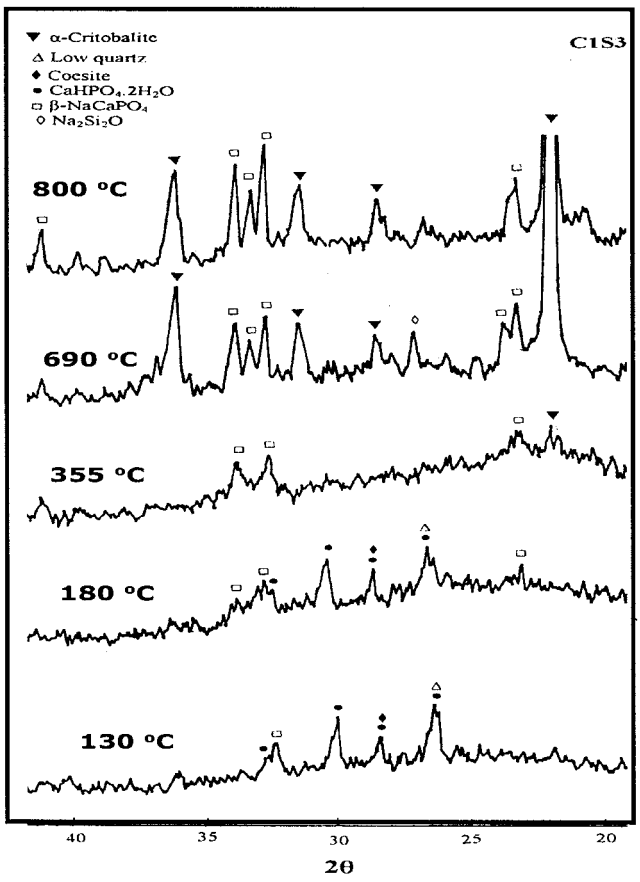

Figure 4. XRD analysis of C1S3 treated at 130° or 180°C showed ill crystallization and comprised brushite ($CaHPO_4$), L-quartz (SiO2) ss and rhenanite (β-$NaCaPO_4$) ss. After treatment at 355°C, $CaHPO_4$ transformed into β-$NaCaPO_4$ ss, and low quartz ss transformed into α-cristobalite ss. The intensity of the signal characteristic of β-$NaCaPO_4$ ss and α-cristobalite ss increased, after treatment at 690° and 800°C, indicating maturation of the crystallization of these two phases.

the main characteristic peaks of α-cristobalite, in all samples, was slightly shifted to a higher value indicating formation of solid solution. The intensity of the signal characteristic of β-$NaCaPO_4$ ss and α-cristobalite ss increased, after treatment at 690°C, indicating maturation of the crystallization of these two phases. In addition, a minor signal indicative of $Na_2Si_2O_5$ was evident. After treatment at 800°C, XRD analysis showed increased crystallization of β-$NaCaPO_4$ ss and α-cristobalite ss (Fig. 4).

C1S1

After treatment at 130°C for 2 h, XRD analysis (Fig. 5) showed that C1S1 samples were composed of $CaHPO_4$ and L-quartz ss. The signals characteristic for β-$NaCaPO_4$ ss were demonstrated after treatment at 180°C. Raising the treatment temperature to 355°C resulted in the decomposition of $CaHPO_4$ into γ-$Ca_2P_2O_7$ ss, β-$Ca_3(PO_4)_2$ ss and β-$NaCaPO_4$ ss. In addition, there was a small signal characteristic of α-cristobalite ss. Samples treated at 690°C composed mainly of β-$NaCaPO_4$ ss and α-cristobalite ss. The crystallization of the latter two phases increased after treatment at 800°C as indicated by the increase in the intensity of their corresponding signals (Fig. 5).

C3S1

XRD analysis of C3S1 treated at 130°C (Fig. 6) showed the characteristic signals of $CaHPO_4$ and L-quartz ss. After treatment at 180°C, signals characteristic of β-$NaCaPO_4$ ss were detected. Raising the treatment temperature to 355°C resulted in a complete

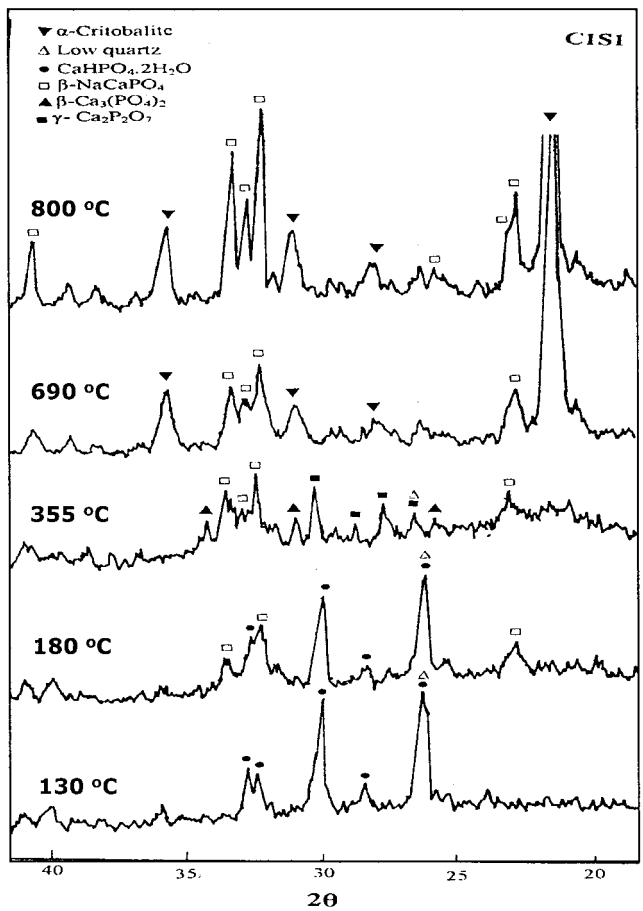

Figure 5. XRD analysis of C1S1 samples treated at 130°showed characteristic signals of $CaHPO_4$ and L-quartz ss. After treatment at 180°C, the signals characteristic for β-$NaCaPO_4$ ss were demonstrated. Raising the treatment temperature to 355°C resulted in the decomposition of $CaHPO_4$ into γ- $Ca_2P_2O_7$ ss, β-$Ca_3(PO_4)_2$ss, and β-$NaCaPO_4$ ss. In addition, there was a small signal characteristic of α-cristobalite ss. Samples treated at 690°C composed mainly of β-$NaCaPO_4$ ss and α-cristobalite ss. The latter two phases increased after treatment at 800°C as indicated by the increase in the intensity of their characteristic signals.

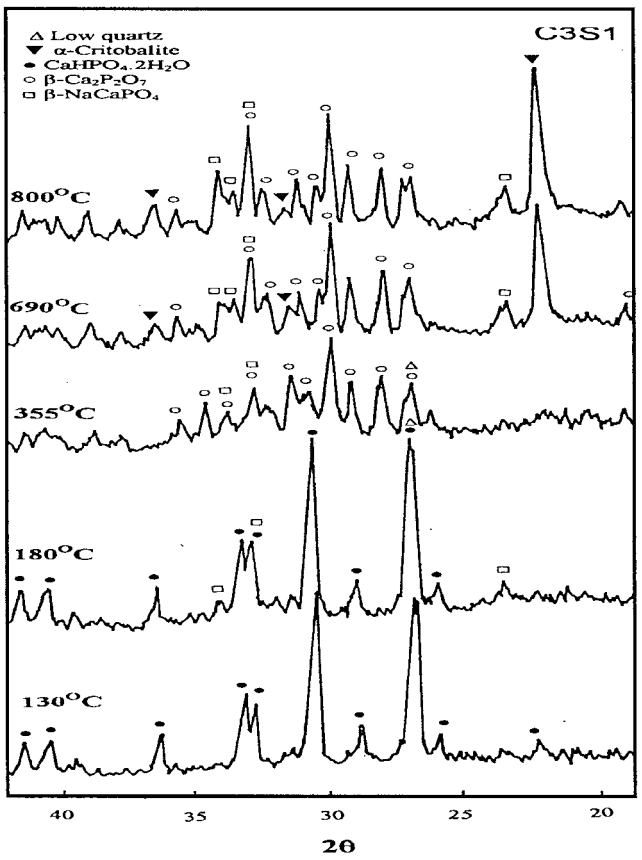

Figure 6. XRD analysis revealed that after treatment at 130°C, C3S1 comprised $CaHPO_4$ and L-quartz ss. As the treatment temperature was raised to 180°C, signals characteristics of β-$NaCaPO_4$ ss were detected. Raising the treatment temperature to 355°C resulted in complete decomposition of $CaHPO_4$ into β-$Ca_2P_2O_7$ ss, β-$Ca_3(PO_4)_2$ss (Whitlockite), and β-$NaCaPO_4$ ss. Whitlockite ss and L-quartz ss decomposed after treatment at 690°and the sample comprised mainly β- $Ca_2P_2O_7$ ss, β-$NaCaPO_4$ ss and α-cristobalite ss. The intensity of the signals characteristic of β-$NaCaPO_4$ ss and α-cristobalite ss increased after treatment at 800°C indicating increased crystallization of these two phases. However, the signals characteristic of β-$Ca_2P_2O_7$ ss were persistent.

decomposition of $CaHPO_4$ into β-$Ca_2P_2O_7$ ss, β-$Ca_3(PO_4)_2$ ss (Whitlockite), and β-$NaCaPO_4$ ss. Whitlockite ss and L-quartz ss decomposed after treatment at 690°C and the sample comprised mainly β-$Ca_2P_2O_7$ ss, β-$NaCaPO_4$ ss, and α-cristobalite ss. The intensity of the signals characteristic of β-$NaCaPO_4$ ss and α-cristobalite ss increased after treatment at 800°C indicating increased crystallization of these two phases. However, the signals characteristic of β-$Ca_2P_2O_7$ ss were persistent.

Scanning electron microscopy

Figure 7 is a SEM micrograph demonstrating the porosity of the silica-calcium phosphate (C3S1) pretreated at 355°C. The pore size ranged from 10–300 μm. Mercury intrusion analysis showed that the porosity percent decreased in the order C1S3 (51%) > C1S1 (47%) > C3S1 (43 %).

Quantitative protein analysis

Total protein analysis showed that all SCPC samples adsorbed a significantly higher amount of serum protein than BG ($p < 0.0001$) (Fig. 8). Comparison among the SCPC samples revealed that protein adsorption was dependent on the chemical composition and crystalline structure. Silica-rich C1S3 adsorbed significantly higher amounts of serum protein than calcium phosphate-rich C3S1 ($p < 0.003$). Protein adsorption onto C3S1, C1S1, and C1S3, pretreated at 130°C, was significantly higher than that adsorbed onto corresponding samples pretreated at either 355 or 690°C. However, all SCPC pretreated at 800°C adsorbed a significantly higher amount of protein than their equivalent samples treated at 690°C ($p < 0.003$).

Corrosion

ICP analysis indicated a significantly higher corrosion rate of SCPC compared to BG (Fig. 9). The amount of Si released from C1S3 into physiological solution was significantly higher than that released from BG at all time periods ($n = 3$, $p < 0.001$). Moreover, Si released from C1S3 increased in the period 0–4 day in the order 0–1 < 1–2 < 2–4 days ($p < 0.05$). On the other hand, comparable Si concentrations were

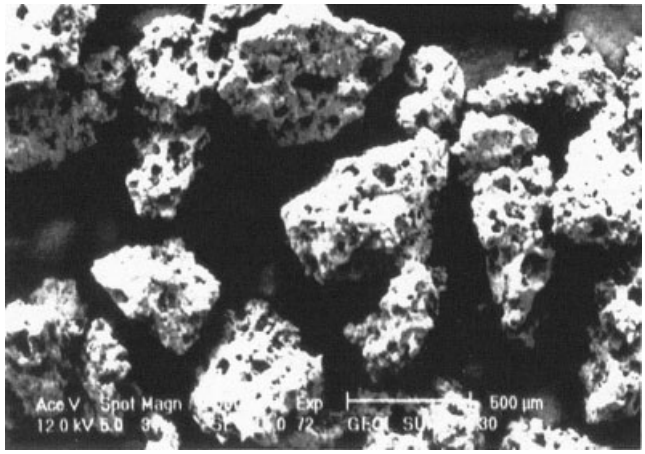

Figure 7. SEM micrograph demonstrating the porosity of the silica-calcium phosphate (C3S1) sample pretreated at 355°C. The material is highly porous with a pore size range from 10–300 μm. Mercury intrusion analysis showed that the porosity percent decreased in the order C1S3 (51%) > C1S1 (47%) > C3S1 (43 %).

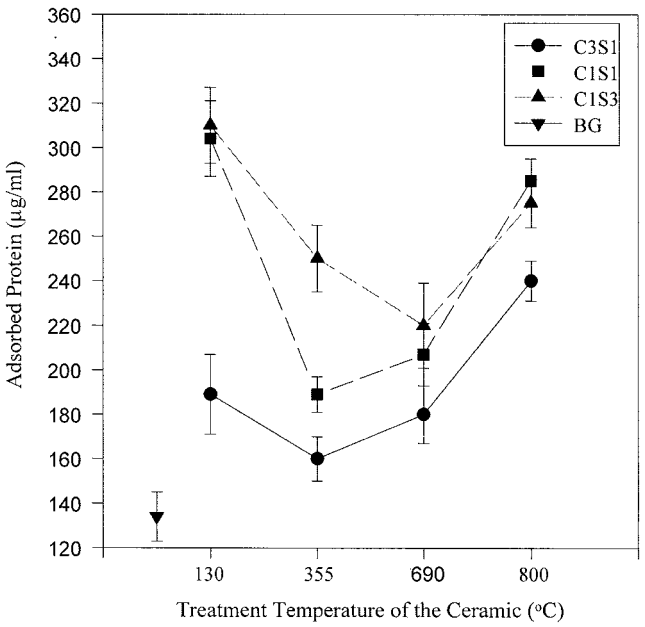

Figure 8. Total protein analysis showed that SCPC adsorbed significantly higher amount of serum protein than bioactive glass ($p < 0.00001$). Silica-rich C1S3 adsorbed significantly higher amounts of serum protein than calcium phosphate-rich C3S1 ($p < 0.003$). Protein adsorption onto C3S1, C1S1, and C1S3, pretreated at 130°C, was significantly higher than the corresponding adsorption onto samples pretreated at either 355° or 690°C. However, all SCPC pretreated at 800°C adsorbed significantly higher amount of protein than their corresponding samples treated at 690°C ($p < 0.003$).

measured in solutions incubated with C1S3 particles for 4, 6, or 8 days. Si concentration released form BG after 2 days was higher than that released after 1 day. However, the difference was not statistically significant. In addition, similar Si concentrations were measured in solutions incubated with BG particles for 2, 4, 6, or 8 days.

Histology

After 3 weeks, defects grafted with C1S3 were almost completely filled with new bone [Fig. 10(a)]. Bone formed in the internal side of the defect has been completely remodeled and few vascular cavities remained. These results indicate that SCPC containing a high silica concentration not only stimulate bone cell function and tissue formation but also resorb in harmony with the new bone tissue formation. New bone is also present within the marrow cavity that was initially filled with graft material. The architecture of the remodeled cortical bone and marrow resembles that of normal healthy bone. This indicates that C1S3 material has a strong stimulatory effect on stem cell differentiation into osteoblasts. EDX analysis (data not shown) of non-decalcified sections of the new bone that formed inside the defect indicates that it is mineralized bone with a Ca/P ratio of 1.65. In defects grafted with C3S1, new bone tissues were seen filling the inter-space between the particles [Fig. 10(b)]. In addition, new bone filled the inner pores of the particles [arrows in Fig. 10(b)] indicating that bone cells colonized the porous structure and deposited bone tissue inside the material. Defects filled with BG were filled with new bone tissue. However, a substantial quantity of graft material was found unresorbed [Fig. 10(c)].

DISCUSSION

We have synthesized a new resorbable porous bioactive silica-calcium phosphate composite that has the ability to adsorb high quantities of serum protein and stimulate rapid bone generation. The superior bioactivity and resorbability of the new SCPC were induced by enforcing ion substitution and development of solid solutions employing thermal treatment. Formation of solid solutions lowered the crystallization temperature of both silica and calcium phosphate and, hence, enhanced their bioactivity. Thus, β-$NaCaPO_4$ started to crystallize at 180°C and continued to grow as the treatment temperature increased up to 800°C. All SCPC samples were superior to BG in terms of protein adsorption, enhancement of bone generation, and graft material resorption. The excellent resorbability of the SCPC compared to BG has been confirmed by corrosion analysis in physiological solution. The high porosity of the SCPC enhanced tissue ingrowth and graft material resorption inside bone defect. The new SCPC may be used for a wide variety of applica-

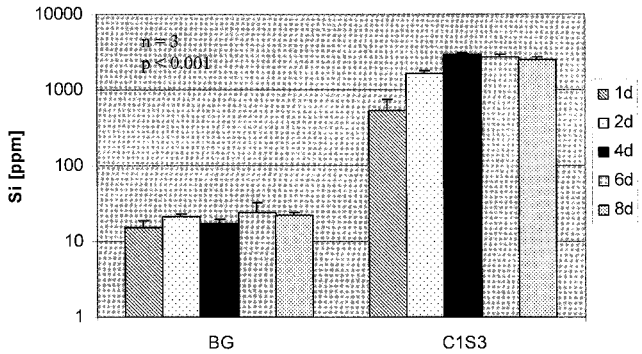

Figure 9. ICP measurements of Si concentration released from SCPC and BG into tissue culture medium containing 10% serum. The amount of Si released from C1S3 was significantly higher than that released from BG at all time periods ($n = 3$, $p < 0.001$), which indicates that the rate of biodegradation of SCPC is significantly higher than that of BG.

tions in the field of bone reconstruction including tissue engineering scaffolds for cell and drug delivery.

DTA, DTGA, and XRD analyses were employed to study the effect of chemical composition and thermal treatment on the crystalline structure and phase transformation in the silica-calcium phosphate composite. DTA-DTGA analyses showed that the endothermic peak at 130°C was accompanied by a major weight loss indicating dehydration of the SCPC. Moreover, as the silica component increased, the area under the peak at 130°C (Fig. 2) was increased due to the loss of water of hydration associated with the silica component. In addition, XRD analyses suggested that, in the silica-rich SCPC samples, the dehydration process was accompanied by limited atomic rearrangements that resulted in the formation of β-$NaCaPO_4$ ss and L-quartz ss. In the calcium phosphate-rich samples, XRD signals characteristic of β-$NaCaPO_4$ ss started to appear only after thermal treatment at 180°C which indicates that the initial phase transformation is highly dependent on the chemical composition. The formation of β-$NaCaPO_4$ ss can be represented by the equation:

$$2CaHPO_4 + Na_2O \rightarrow 2\ \beta\text{-}NaCaPO_4\ (ss) + H_2O \quad (1)$$

The DTA peak recorded at 355°C is indicative of two phase-transformation reactions that could be represented by the following equations:

$$4\ CaHPO_4 \rightarrow 2\ Ca_2P_2O_7\ (ss) + 2H_2O \quad (2)$$

$$CaHPO_4 + Ca_2P_2O_7\ (ss) \rightarrow$$

$$\beta\text{-}Ca_3(PO_4)_2\ (ss) + \tfrac{1}{2}\ P_2O_5 + \tfrac{1}{2}\ H_2O \quad (3)$$

It is interesting to note that while the characteristic XRD signals for $Ca_2P_2O_7$ ss and β-$Ca_3(PO_4)_2$ ss were evident for C3S1 and C1S1, these signals were greatly diminished in the spectra of C1S3 due to the presence of low content of calcium phosphate component in this sample. It is for the same reason that the area under the DTA peak at 355°C was minimal for C1S3 sample. These results suggest that the early transformation of $CaHPO_4$ into β-$NaCaPO_4$ ss (eq 1) in C1S3

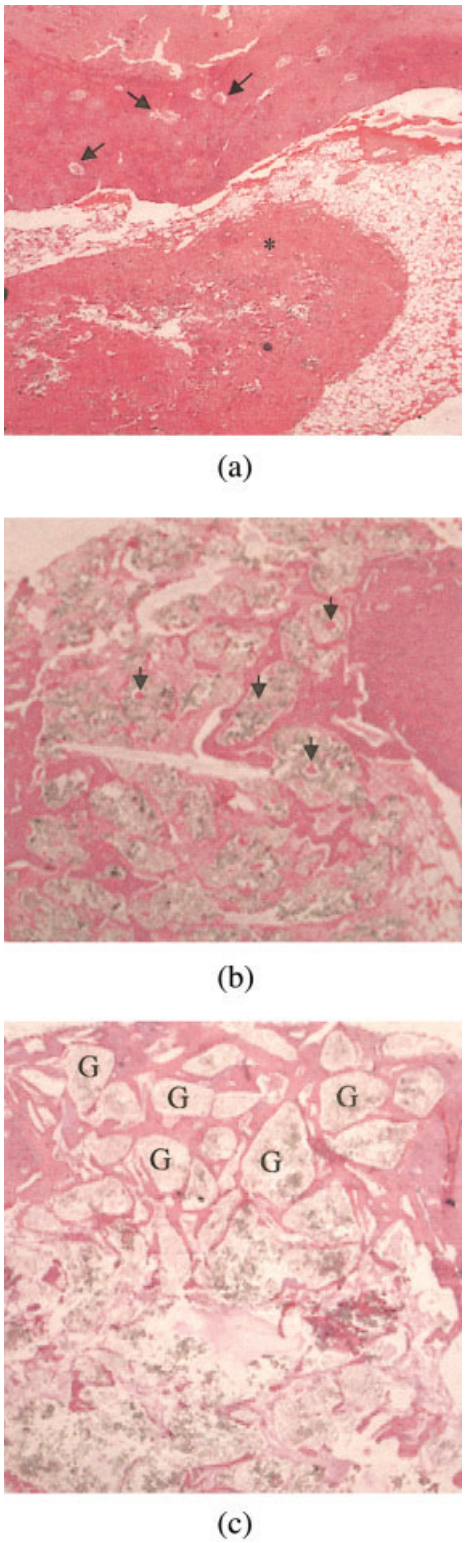

Figure 10. Histology analysis of critical size bone defect created in the rabbit femur and grafted with C3S1, C1S3, or BG. After 3 weeks, defects grafted with C1S3 were almost completely filled with new bone (a). Bone formed in the internal side of the defect has been completely remodeled and few vascular cavities (arrows) remained. New bone (*) is also present within the marrow cavity that was initially filled with graft material. The architecture of the remodeled cortical bone and marrow resembles that of normal healthy bone. In defects grafted with C3S1 (b), new bone tissues were seen filling the inter-space between the particles as well as inside the pores (arrows). Defects filled with BG were filled with new bone tissue; however, a substantial quantity of graft material (G) was found unresorbed (c) (H&E ×40). [Color figure can be viewed in the online issue, which is available at www.interscience.wiley.com.]

minimizes the amount of $CaHPO_4$ available for carrying out the reaction represented by equations (2) and (3). The phase transformation reactions (in eqs 2 and 3) were accompanied by release of H_2O and P_2O_5, which could be responsible for the observed two-step weight losses, noted in the DTGA thermogram of C3S1, in the temperature range 206–489°C. Moreover, the release of H_2O and P_2O_5 represented by equations 1, 2, and 3 contributes to the formation of pores inside the ceramic matrix as shown in SEM analysis (Fig. 7).

It should be noted that β-$Ca_3(PO_4)_2$ ss and $Ca_2P_2O_7$ ss were formed at a significantly lower temperature than that reported in the literature. Boullè and Rabatin et al. reported that the transformation of $CaHPO_4$ into $Ca_2P_2O_7$ takes place at about 430°C.[30,31] Moreover, the formation of β-$Ca_3(PO_4)_2$by the reaction of $CaHPO_4$ with $CaCO_3$ or the reaction of the $Ca_2P_2O_7$ with CaO is usually carried out at 1,000°C.[32] In the absence of CaO, the transformation of $Ca_2P_2O_7$ into β-$Ca_3(PO_4)_2$takes place at 1,800°C.[33] One possible reason for the formation of β-$Ca_3(PO_4)_2$ss at this low temperature is the impurity of the system represented by Na and Si ions. These impurities usually result in the development of solid solutions and crystal defects. Indeed, the development of solid solutions has been confirmed by the slight shifts in the 2θ values of the characteristic signals of both silica and calcium phosphate crystalline phases. In addition, we speculate that the heat evolved from the exothermic acid-base reactions in the system would facilitate the formation of β-$Ca_3(PO_4)_2$ss and $Ca_2P_2O_7$ ss at a low temperature. Likewise, XRD analysis of the Si-rich calcium phosphate composite C1S3 indicated that L-quartz ss transformed into α-cristobalite ss at a significantly lower temperature (355°C) than that reported in the literature (1,470°C).[34] The direct transformation of L-quartz ss into α-cristobalite ss could be enhanced by the formation of solid solution and by the heat liberated during the transformation of $CaHPO_4$ into β-$NaCaPO_4$ ss.

XRD signals characteristic of the β-$NaCaPO_4$ ss increased in all samples after thermal treatment at 690 and 800°C. On the other hand, XRD signals characteristics β-$Ca_3(PO_4)_2$ss totally disappeared and those characteristics of $Ca_2P_2O_7$ ss were significantly reduced. Therefore, the two endothermic peaks appeared at 690°and 800°C (Fig. 2) can be assigned to the interaction of $Ca_2P_2O_7$ss and β-$Ca_3(PO_4)_2$ss with Na_2O as follows,

$$Ca_2P_2O_7\ (ss) + Na_2O \rightarrow 2\ \beta\text{-}NaCaPO_4\ (ss) \quad (4)$$

$$\beta\text{-}Ca_3(PO_4)_2\ (ss) + Na_2O \rightarrow 2\ \beta\text{-}NaCaPO_4\ (ss) + CaO \quad (5)$$

The stability of pyrophosphate in the calcium phosphate-rich composite C3S1 could be attributed to the presence of insufficient Na_2O to carry out the reaction represented by equations (4 and 5).

In conjunction with the phase transformation of both the silica and the calcium phosphate components, there were significant changes in serum protein adsorption. The transformation of $CaHPO_4$ into $Ca_2P_2O_7$ ss and β-$Ca_3(PO_4)_2$ss significantly inhibited protein adsorption. The enhanced protein adsorption on $CaHPO_4$ could be attributed to the high ratio of Ca-to-P sites on the material surface.[35] On the other hand, the inhibition of protein adsorption onto the surface of pyrophosphates and tricalcium phosphate is due to the low ratio of Ca-to-P and high surface negativity of $[P_2O_7]^{4-}$ and $[(PO_4)_2]^{6-}$, respectively. The increase in surface negativity of the material makes adsorption of negatively charged glycoprotein molecules a thermodynamically unfavorable reaction ($\Delta G>0$).[36] On the other hand, as $Ca_2P_2O_7$ ss transformed into β-$NaCaPO_4$ ss serum protein adsorption was enhanced. The affinity of β-$NaCaPO_4$ ss towards serum protein would be higher than that of $Ca_2P_2O_7$ss due to the presence of labile Na atom in the former compound. Protein adsorption was also significantly controlled by the crystallization and phase transformation of the silica phase(s). In all composites, the crystallization of amorphous silica inhibited protein adsorption. However, the degree of inhibition varied depending on the concentration and nature of the crystalline silica phase. Composites that contained α-cristobalite ss adsorbed a significantly higher amount of serum protein than those contained L-quartz ss. The enhancement of protein adsorption correlates well with the fact that α-cristobalite ss has a comparatively open atomic structure, whereas the atoms in quartz are more closely linked.[34] Moreover, α-cristobalite ss is characterized by a tetragonal structure, with less degree of symmetry than the hexagonal structure of low quartz ss. Therefore, in biological solutions, α-cristobalite ss becomes more polar than L-quartz ss and can easily bind to the active sites of the protein molecule. In addition, the formation of crystal defects and solid solutions is expected to increase after treatment at high temperature (800°C), which further activates the material by providing charged surface sites favorable for protein binding. It is also possible that the surface characteristics of SCPC dictate a favorable protein conformation that enhances cell–material interaction and tissue integration. A more detailed study is currently underway in order to understand the actual submolecular level mechanisms involved in adsorption behavior.

When implanted in bone, SCPC showed an osteoconductive effect superior to that of BG. After 3 weeks, bone defects grafted with C1S3 were filled with bone tissue incorporating minimal residues of graft mate-

rial. These results indicate that SCPC containing high silica concentrations not only have a strong stimulatory effect on bone cell function but also resorb in harmony with the rate of new bone formation. New bone was also present within the marrow cavity that was initially filled with graft material. The architecture of the remodeled cortical bone and marrow resembles that of normal healthy bone. This indicates that C1S3 material has a strong stimulatory effect on stem cell differentiation into bone-forming cells (osteoblasts). The superior bioactivity and resorbability of the Si-rich calcium phosphate ceramic are due to the physicochemical properties of its mineral constituents. β-$NaCaPO_4$ ss contains Na ions that weaken the bond between Ca^{2+} and the PO_4^{3-} in the crystal surface and, hence, facilitate dissolution. Previous studies reported that β-$NaCaPO_4$ has improved bioactivity compared to hydroxyapatite due to its higher rate of solubility in the body.[37,38] In addition, because of its enhanced solubility, β-$NaCaPO_4$ ss can act as a weak interphase for α-cristobalite ss and provide an easy path for structure debonding, which facilitates silica dissolution as demonstrated in (Fig. 9). In conjunction with the enhanced silica release, rapid bone regeneration was observed, which suggests that SCPC promoted bone generation by releasing a substantial concentration of soluble silicon inside bone defects. Previous studies reported that soluble silicon may be responsible for the increased metabolic activity of bone cells.[39,40] It should be noted that BG enhanced bone formation but showed very limited resorbability compared to SCPC samples. In conjunction with the low restorability of BG *in vivo*, we observed a restricted material dissolution *in vitro*. ICP analyses indicated that the rate of Si dissolution of C1S3 is significantly higher than that of BG (Fig. 9). The poor resorbability of BG is connected to the formation of a silica-rich layer on the material surface, which hinders ion diffusion from the glass bulk into the surface and hence limits solubility. Another factor that contributes to the low resorbability of BG is its dense structure that provides limited surface area in contact with tissue fluids and cells. On the other hand, the high porosity of SCPC has provided high surface area in contact with tissue fluids and cells, which enhanced resorbability and new bone tissue formation.

As bonds between Ca^{2+} and PO_4^{3-} in β-$NaCaPO_4$ ss are weaker than the corresponding bonds between Ca^{2+} and the $P_2O_7^{4-}$ in the $Ca_2P_2O_7$ ss, it is expected that the solubility of $Ca_2P_2O_7$ ss would be lower than that of β-$NaCaPO_4$ ss. Therefore, the relatively low resorbability of C3S1 compared to C1S3 could be attributed to the presence of high content of pyrophosphate in the former material. Other studies showed that the dissolution of pyrophosphate is comparable to those of hydroxyapatite and fluorapatite.[41,42] Studies are currently underway to analyze the corrosion behavior of SCPC and evaluate its ability to serve as a delivery vehicle for BMP-2 and mesenchymal stem cells.

CONCLUSION

A major achievement in this study is that we synthesized a new resorbable porous bioactive silica-calcium phosphate composite that has the ability to adsorb high quantities of serum protein and stimulate rapid bone generation. The high porosity of the SCPC enhanced cell colonization and bone formation on and within the graft material. The bone conductive effect and resorbability of SCPC were not limited by ion diffusion and, hence, were superior to those of BG. The high rate of silica dissolution from SCPC promoted rapid bone regeneration and graft material resorption. Thermal treatment of the SCPC induced ion substitution and formation of solid solutions at significantly low temperature. These ultrastructural modifications facilitated protein adsorption and controlled SCPC solubility. SCPC comprised β-$NaCaPO_4$ ss enhanced bone regeneration and material resorption better than that containing $Ca_2P_2O_7$ ss. The excellent bioactivity and high porosity of the SCPC suggest that this material can be used as a vehicle for cell and drug delivery. Moreover, the material could be applied as a coat on metallic implants to enhance implant fixation and can be mixed with polymers to promote its bioactivity.

References

1. Chapekar MS. Tissue engineering: challenges and opportunities. Biomed Mater Res 2000;53:617–620.
2. Praemer A, Furner S, Rice DP. Musculoskeletal conditions in the United States. Proceedings of the American Academy of Orthopaedic Surgeons. Park Ridge, IL. 1992;83–124.
3. Reeve J, Metz D. Age Net workshop on ageing fragility and the biomechanics of bone. AgeNet Rep 1998;1–3.
4. Damien CJ, Parsons JR. Bone graft and bone graft substitutes: a review of current technology and applications. J Appl Biomater 1991;2:187–208.
5. Glowacki J, Mulliken JB. Demineralized bone implants. Clin Plast Surg 1985;12:233–233.
6. Buck BE, Malinin TI, Brown MD. Bone transplantation and human immunodeficiency virus. An estimate of risk of aquired immunodeficiency syndrome (AIDS). Clin Orthop Rel Res 1989;240:129–136.
7. Oreffo RO, Triffitt JT. Future potentials for using osteogenic stem cells and biomaterials in orthopedics. Bone 1999;25:5S–9S.
8. Horisaka Y, Okamoto Y, Matsumoto N, Yoshimura Y, Kawada J, Yamashita K, Takagi T. Implantation of bone morphogenetic protein adsorbed to hydroxyapatite. Clin Orthop 1991;268:303–312.
9. Doll BA, Towle HJ, Hollinger JO, Reddi AH, Mellonig JT. The osteogenic potential of two composite graft systems using osteogenin. J Periodontol 1990;61:745–750.

10. Schepers E, de Clercq M, Ducheyne P, Kempeneers R. Bioactive glass particulate material as a filler for bone lesions. J Oral Rehabil 1991;18:439–445.
11. Eggli PS, Muller W, Schenk RK. Porous hydroxyapatite and tricalcium phosphate cylinderswith two different pore size rangesimplanted in the cancellous bone of rabbits. Clin Orthop 1988;232:127–137.
12. Ogino M, Ohuchi F, Hench LL. Compositional dependence of the formation of calcium phosphate films on bioglass. J Biomed Mater Res 1980;14:55–64.
13. Klein CPAT, Dreissen AA, de Groot K, van den Hooff A. Biodegradation behavior of various calcium phosphate materials in bone tissue. J Biomed Mater Res 1983;17:769–784.
14. El-Ghannam A, Ducheyne P, Shapiro IM. Serum protein adsorption on bioactive ceramics and glasses and the effect on osteoblast adhesion. The 21st Annual Meeting of the Society for Biomaterials, San Francisco, CA, March 1995.
15. El-Ghannam A, Ducheyne P, Shapiro IM. Effect of serum proteins on osteoblast adhesion to surface modified bioactive glass and hydroxyapatite. J Orthop Res 1999;17:340–345.
16. García AJ, Ducheyne P, Boettiger D. Effect of surface reaction stage on fibronectin-mediated adhesion of fibroblast-like cells to bioactive glass. J Biomed Mater Res 1998;40:48–56.
17. Oonishi H, Yasukawa E, Iwaki H, Hench LL, Wilson J, Tsuji E, Sugihara T. Particulate Bioglass compared with hydroxyapatite as a bone graft substitute. J Clin Orthop Rel Res 1997;334: 316–325.
18. Fujishiro Y, Oonishi H, Hench LL. Quantitative comparison of in vivo bone generation with particulate Bioglass and hydroxyapatite as a bone graft substitute. In: Sedel L, Rey C, editors. Bioceramics 10. New York: Elsevier; 1997. p 283–286.
19. Furusawa T, Mizunuma K, Yamashita S, Takahashi T. Investigation of early bone formation using resorbable bioactive glass in the rat mandible. Int J Oral Maxillofac Implants 1998;13:672–676.
20. Grenga TE, Zins JE, Bauer T. The rate of vascularization of coralline hydroxyapatite. Plast Reconstr Surg 1989;84:245–249.
21. Schliephake H, Neukam FW, Klosa D. Influence of pore dimensions on bone ingrowth into porous hydroxyapatite blocks used as bone graft substitutes: An isometric study. Int J Oral Maxillofac Surg 1991;20:53–58.
22. Tancred DC, McCormack BA, Carr AJ. A synthetic bone implant macroscopically identical to cancellous bone. Biomaterials 1998;19:2303–2311.
23. Hench LL. Bioceramics: From concept to clinic. J Am Ceram Soc 1991;74:1487–1510.
24. Anderson OH, Kangasniemi L. Calcium phosphate formation at the surface of bioactive glass in vitro. J Biomed Mater Res 1991;25:1019–1030.
25. Hench LL, Andersson OH. Bioactive glasses. In: Hench L, Willson J, editors. An introduction to bioceramics. Singapore: World Scientific; 1993. p 41–62.
26. Fllugieras RM, LaTorre G, Hench LL. Solution effects on the surface reactions of a bioactive glass. J Biomed Mater Res 1993;27:445–453.
27. Li P, Ohtusuki C, Kokubo T, Nakanishi K, Soga N, Nakamura T, Yamamuro T. Effects of ions in aqueous media on hydroxyapatite induction by silica gel and its relevance to bioactivity of bioactive glasses and glass-ceramics. J Appl Biomater 1993;4: 221–229.
28. Shapoff CA, Alexander DC, Clark AE. Clinical use of a bioactive glass particulate in the treatment of human osseous defects. Compendium 1997;18:352–363.
29. Hench LL. Stability of ceramics in the physiological environment. In: Williams DF, editor. Fundamental aspects of biocompatibility. Boca Raton, FL: CRC Press; 1981. p 67–85.
30. Boullè A. Dehydration of calcium phosphate. Silicium, Schwefel, Phosphate, Colloq Sek Aanorg Chem Intern 1954; 217–224.
31. Rabatin JG, Gale RH, Newkirk AE. The mechanism and kinetics of the dehydration of calcium phosphate dihydrate. J Phys Chem 1960;64:491–493.
32. Macarovici D. Phosphates I. Reactions of the synthesis of tertiary calcium phosphate by the thermal methods. Rev Roumaine Chim 1966;11:725–731.
33. Dzyuba ED, Sokdav MT, Valyukevich LP. Thermal stability of calcium phosphates. Izv Akad Nauk SSSR, Neorg Mater 1982; 18:107–110.
34. Berry LG, Mason B. Mineralogy: concepts, descriptions, and determinations. New York: W. H. Freeman, and Company; 1983. p 394.
35. Ohta K, Monma H, Takahashi S. Adsorption characteristics of proteins on calcium phosphates using liquid chromatography. J Biomed Mater Res 2001;55:409–414.
36. Latour RA Jr, Rini CJ. Theoretical analysis of adsorption thermodynamics for hydrophobic peptide residues on SAM surfaces of varying functionality. J Biomed Mater Res 2002;60: 564–577.
37. Kangasniemi I, Vedal E, de Blick-Hogerworst J, Yli-Urpo AU, deGroot K. Dissolution and scanning electron microscopic studies of Ca, P particle containing bioactive glasses. J Biomed Mater Res 1993;27:1225–1233.
38. Kangasniemi I, deGroot K, Wolk J. The stability of hydroxyapatite in an optimized bioactive glass matrix at sintering temperatures. J Mater Sci 1991;2:133–137.
39. Keeting PE, Oursler MJ, Wiegand KE, Bonde SK, Spelsberg TC, Riggs BL. Zeolite A increases proliferation, diffrentiation, and transforming growth factor β production in normal adult human oseoblast-like cells *in vitro*. J Bone Miner Res 1992;7:1281–1289.
40. Hench LL. Bioactive ceramics: theory and clinical applications. In: Andersson OH, Yli-Urpo A, editors. Bioceramics 7. Oxford: Butterworth-Heinemann Ltd.; 1994. p 3–16.
41. Margaret RC, Jesper D, Jørgen C. Kinetics of growth and dissolution of calcium hydroxyapatite in suspensions with variable calcium to phosphate ratio. J Cryst Growth 1998;186: 283–290.
42. Jorgen C, Margaret RC, Thue J. Some new aspects of surface nucleation applied to the growth and dissolution of fluorapatite and hydroxyapatite. J Cryst Growth 1996;163:304–310.